Research Square

Preprints are preliminary reports that have not undergone peer review.
They should not be considered conclusive, used to inform clinical practice,
or referenced by the media as validated information.

Antifouling Meshes Formation for Excellent Oil-Water Separation

Shimeles T. Bulbula

shimeles.tadesse@astu.edu.et

Adama Science and Technology University

Mesfin Belayneh Ageze

Addis Ababa Institute of Technology, Addis Ababa University

Research Article

Keywords: Water-oil separation, GO and TiO2 nanocomposite, Superoleophobic, Antifouling Meshes

Posted Date: June 4th, 2026

DOI: https://doi.org/10.21203/rs.3.rs-9439537/v1

License: This work is licensed under a Creative Commons Attribution 4.0 International License.
Read Full License

Additional Declarations: No competing interests reported.

Abstract

The rapid development of industries has resulted in the frequent occurrence of oil spills and chemical leakages discharged into water bodies, causing severe environmental pollution and ecological damage. Over the past decade, numerous superhydrophobic and oleophilic materials (such as filter membranes, activated carbon, and hydrogels) have been researched and developed for oil-water separation. However, most oil removal materials are susceptible to contamination or blockage during the permeation of oils through the membrane or mesh, highlighting the need for further investigation into effective oil-water separation methods. Currently, there is a pressing need to create nontoxic, efficient, safe, novel, and environmentally friendly antifouling materials and techniques.

In this work, a composite of TiO_2 and GO is proposed to coat stainless steel meshes via a chemical method, creating an underwater superoleophobic mesh with antifouling properties to realize efficient oil-water separation. Results demonstrated that the composite GO/TiO_2 coated mesh not only shows excellent oil-water mixture separation but also exhibits long-term anti-fouling properties. Hence, we conclude that this separation material would be a great contribution to future advanced technology.

Introduction

Water is fundamental for all living things. In fact, water plays a high-impact role in food security, urbanization, public health, and energy production. However, with rapid industrial development and expansion, the frequent occurrence of oil spills and chemical leakages discharged into water bodies has caused severe environmental pollution and ecological damage.(Munirasu, Haija et al. 2016, Bulbula, Dong et al. 2018) Thus, water purification has become one of the major global issues.

Over the past decade, various superhydrophobic and oleophilic materials (such as filter membranes, kapok, activated carbon, and hydrophobic aerogels) have been explored and developed for oil-water separation, owing to their advantageous gravity-driven properties.(Wen, Di et al. 2013, Zhu, Chen et al. 2017, Liu, Lu et al. 2021) However, these oil removal materials often become contaminated or clogged during the permeation of oils through the membrane or mesh. Consequently, additional research is required to develop advanced materials or techniques for improved oil-water separation.(Mir, Naderifar et al. 2022)

Recently, materials exhibiting oil-repellent properties in aqueous media have garnered significant interest. Drawing inspiration from this technique, several underwater superoleophobic materials have been developed, demonstrating performance akin to fish scales for oil-water separation, including pH-responsive polymers,(Reyes-Ortega 2014) hydrogels, and zeolite based coated meshes.(Wen, Di et al. 2013, Wang, Li et al. 2023) Y. Dong et al. reported that graphene oxide with a layered nanostructure was developed for building effective underwater superoleophobic films.(Dong, Li et al. 2014) The advantage of applying a GO solution to the mesh stems from the layered structure of GO, which is decorated with various oxygen-containing functional groups, including carboxyl and hydroxyl groups, on both the basal

plane and the edges. These functional groups improve the dispersion of GO in various polar solutions and impart excellent hydrophilic properties.

However, mesh fouling is a persistent challenge that limits performance efficiency by decreasing water permeation flux, which in turn deteriorates both the quality and quantity of product water. Typically, mesh fouling can result from pore blocking, cake formation, organic adsorption, inorganic precipitation, and biological fouling, all of which can cause either temporary or permanent declines in flux.(Xue, Wang et al. 2011, Dong, Li et al. 2014) Therefore, mesh fouling poses a significant challenge in various water purification applications, including industrial and municipal wastewater treatment, as well as the production of ultra-pure and potable water.

To address the issue of mesh fouling, several strategies have been implemented, including the pre-treatment, mesh cleaning, optimization of operational conditions, and the development of antifouling meshes.(Jo and Kim 2016, Liu, Hou et al. 2017) Today, there is an urgent and critical need to develop nontoxic, efficient, safe, novel, and environmentally friendly antifouling materials and techniques. This necessity arises from the imbalance between demand and supply resulting from insufficient water quantity and quality. While mesh cleaning methods (such as physical cleaning, chemical washing, or the application of photon energy) are straightforward, effective, and widely used to remove foulants, they can lead to the degradation of the mesh matrix materials.(Panda and De 2015) In recent years, photocatalytic techniques have been widely investigated due to their considerable potential for mineralizing organic pollutants, disinfecting water and air, producing renewable fuels, and facilitating organic synthesis. (Baek, Kim et al. 2014, Liu, Hou et al. 2017) In particular, semiconductor materials like TiO_2, CdSe, and CdTe serve as effective photocatalysts due to their advantageous light absorption properties, rapid charge transport characteristics, and prolonged excited-state lifetimes. Among these, TiO_2 has been the most extensively studied material because of its self-cleaning capabilities, chemical stability, antibacterial properties, and high photocatalytic activity in removing pollutants from water.(Xu, Xu et al. 2014, Kang, Cheng et al. 2018, Nascimben Santos, Agoston et al. 2020, Meng, Li et al. 2026). Therefore, here the composition of TiO_2 and GO is proposed to coat on stainless steel meshes to prepare underwater superoleophobic mesh with antifouling properties to realize efficient oil-water separation. Results demonstrated that the GO/TiO_2 coated mesh not only shows excellent separation efficiency towards oil-water mixtures, but also exhibited long-term anti-fouling properties.

Materials and Methods

Materials

TiO_2/P25 powder, Graphite powder, H_2SO_4, $NaNO_3$, $KMnO_4$, H_2O_2, HCl, stainless mesh (300 mesh size), oleic acid, hexane, toluene, chloroform, dichloroethane and UV light source.

Preparation of GO/TiO2

Graphite oxide (GO) was synthesized from natural graphite powder employing a modified Hummers and Offeman's method.(Hummers Jr and Offeman 1958) This involved treating the graphite powder with H_2SO_4, $NaNO_3$, and $KMnO_4$.To synthesize GO/P25 (TiO_2) powder was added into a 200 ml graphite oxide solution (3 mg/ml) under stirring at room temperature until a homogeneous solution was formed.

Coating of GO/TiO2 on Stainless Meshes

First, the stainless meshes were carefully washed with ethanol and water, consecutively. Then, the mesh was immersed in a GO/TiO_2 aqueous solution and subjected to mild sonication for 10 minutes. Following this, the coated mesh was dried in an electric oven at 60°C. Finally, the prepared GO/TiO_2 coated mesh was positioned between a conical flask and a glass funnel. A 30 mL oil/water mixture (50% v/v) was then added to the conical flask, and the oil-water separation through the coated mesh was observed. The volume of the separated water was measured.

Fouling and ant-fouling test

The coated mesh was immersed into a graduated beaker which contained 20 ml of an ethanol solution with 10 wt% oleic acid, and it was stirred for 30 minutes. Then, the mesh was dried at 60°C, followed by ethanol washing and drying. Finally, the underwater oil contact angle was measured. After the contact angle was measured, the polluted meshes were immersed into a beaker which contained 20 ml of water, and they were UV irradiated for 1 hour. The meshes were then washed with water, and finally, the underwater contact angle was measured.

Characterization

The crystallographic information was analyzed using powder X-ray diffraction (XRD) with a Bruker D8 Advance, utilizing Cu-Kα radiation at 40 kV and 40 mA. The morphology and structure of the samples were examined with scanning electron microscopy (SEM, Hitachi S4800) and high-resolution transmission electron microscopy. The contact angles were measured by a DATAPHYSICS OCA35 instrument. The elemental mapping was conducted via Energy Dispersive Spectrometer (EDS). The wave nature of APS-GO was performed using Fourier Transform Infrared Spectroscopy (FTIR).

Results and Discussion

The crystal phase of GO, TiO_2/P25, and their composite (GO/TiO_2) were investigated by XRD patterns (Fig. 1).As shown in the XRD pattern, the anatase phase of P25 diffraction peaks was observed at the 2θ values of 25.2, 37.9, 48.2, 55.3, 53.9, 62.6, 69.3, 70.2, 75.3, and 76.2°, corresponding to the diffraction planes of (1 0 1), (0 0 4), (2 0 0), (2 1 1), (1 0 5), (2 0 4), (1 1 6), (2 2 0), (2 1 5), and (3 0 1), respectively. The rutile phase of P25 with diffraction peaks at 27.5, 36.3, 54.5, and 62.6° were observed, corresponding to the diffraction planes of (1 1 0), (1 0 1), (2 1 1), and (3 1 0) [JCPDS Card No. 86-1156],

respectively. After the GO/TiO_2 composite was formed, a new diffraction peak pattern was observed at 2θ = 10.8, with a corresponding interlayer spacing of 0.81 nm, as indicated by the GO pattern. Some diffraction peak patterns of P25 were still present.

The SEM (a) and HRTEM (b-e) of the GO/TiO_2 mixture are shown in Fig. 2. The GO and TiO_2 binding layer interface can be easily distinguished (Fig. 2a). As shown in Figs. 2(b, c, d, and e), TiO_2 particles are found on top of the graphene sheets, and the individual particle size is nearly about 20 nm. Furthermore, the lattice fringes are 0.35 nm (Fig. 2f), which agrees with the anatase titania (101) interplanar spacing.(Lu, Cheng et al. 2018) The SEM image of the neat pure stainless steel meshes is shown in Fig. 2g, with an average pore diameter of about 37 µm. The SEM image of the GO/TiO_2 coated stainless steel mesh with different image magnifications is shown in Figs. 2 (h and i). As shown on the coated mesh, the composite sample is distributed uniformly on the surface of the mesh, and the neat mesh pores are covered by the GO/TiO_2 mixture.

For further identification of the elemental ratio distribution in the GO/TiO_2 mixture, the element mapping was analyzed. As shown in Figs. 3(a, and b), mainly three elements (C, O, and Ti) were observed. The calculated weight ratio was nearly 32:33:35 percent for C, O, and Ti, respectively.

The possible interactions between TiO_2 and carbon phases were analyzed using FTIR spectra (Fig. 4). The FTIR spectrum recorded for TiO_2 showed a mainly broad band situated from 400 to 800 cm^{-1}, which was attributed to Ti-O stretching and vibration of Ti-O-Ti bonds present in the structure of TiO_2 (Fig. 4, red curve). Additionally, other broad band peaks were observed at 3400 and 1650 cm^{-1}, which were associated with the stretching vibration of the surface-adsorbed water molecules and hydroxyl groups, respectively. As shown in Fig. 4 (black curve), the GO powder sample displays several characteristic features, including a wealth of functional groups such as -OH, -COOH, and -O-. The prominent peak around 3400 cm^{-1} corresponds to -OH groups, which are derived from water, hydroxide, and carboxyl groups.(Yang, Chen et al. 2016) The C = O stretching of the –COOH group is observed at 1725 cm^{-1}, while the O-H bending of C-OH is seen at 1618 cm^{-1}. Additionally, the O-H vibration of the C-OH groups is identified at 1385 cm^{-1}, the C-O vibration of C-OH appears at 1260 cm^{-1}, and epoxy vibrations are detected at 1050 and 975 cm^{-1}, consistent with previous reports.(Sagadevan, Pal et al. 2017) When examining the composite (GO/TiO_2) (Fig. 4, blue curve), the intensity of the spectrum peaks corresponding to GO (such as the C = O stretching of COOH groups, C = C vibrations, C–OH stretching vibrations, and C–O vibrations from alkoxy groups) was significantly reduced. This indicates that the oxygen-containing functional groups in GO were disintegrated. Furthermore, the strong absorption around 450 cm^{-1} is attributed to the vibrational stretching of Ti–O–Ti bonds in TiO_2, confirming the formation of the GO/TiO_2 nanocomposite.(Zhang, Lv et al. 2010, He, Que et al. 2013, Sagadevan, Pal et al. 2017)

As shown in Fig. 5, the camera lens image easily identified the uncoated (Fig. 5a) and coated (Fig. 5b) meshes. The mixture of GO/TiO_2 was uniformly distributed on the surface of the mesh (Fig. 5b). The oil-

water separation image (Figs. 5c and 5d) shows a mixture of hexane and water (50%:50%) prepared in a graduated cylinder. The red dye was used to distinguish the volume boundary of oil and water. The hexane easily covered the upper surface of the cylinder due to its lower density than water. However, due to the existence of coated mesh's excellent superoleophobic properties of the hexane was prevented from permeating through the mesh (Fig. 5d). The wettability of water and oil on the coated meshes was assessed through contact angle measurements. (Fig. 5e). In an air medium, the oil easily covered the coated mesh surface. However, under water, both light and heavy oils had underwater oil contact angles nearly greater than 150°, indicating that the GO/TiO_2 coated mesh exhibited excellent underwater superoleophobic properties.

The separation efficiency was also performed before and after coating the mesh for different oil-water mixtures (Fig. 5f) using the formula ($V_{separation}/V_{initial}$) x 100, where $V_{separation}$ is the volume of water and oil after separation, and $V_{initial}$ is the volume of water and oil before making the mixture. The oil rejection efficiency was excellent, but the water permeation efficiency reduced during denser oil mixtures due to the denser oil easily building up layers to block water flow. This mesh fouling continually serves as a bottleneck that limits performance efficiency by decreasing water permeation flux, which leads to a decline in product water quality. To recover the fouling problem, the coated mesh was treated with a UV light source.

After the polluted meshes were treated by UV, the meshes were recovered, and hence the contact angle rose up (between 148–156°C, Fig. 6(a, and b). Furthermore, after five cycles, the underwater contact angles of Hexane (lighter oil) and dichloroethane (a heavier oil) were still around 150°C, indicating that the anti-fouling properties were successfully recovered. The benefit of the GO layer is its decoration with various oxygen-containing functional groups, and TiO_2 is the most intensively self-cleaning, chemical stability, and photocatalytic activity. This makes

the GO/TiO_2 coated mesh nontoxic, efficient, safe, not-expensive, and environmentally friendly antifouling materials for removing pollutants from water.

Declarations

Ethical Approval

Not applicable.

Conflicts of interest

there are no conflicts to declare.

Funding

This research was financially supported by the Chinese Government Scholarship and the Ethiopian Ministry of Education.

Author Contribution

Shimeles T. Bulbula: Conceptualized the idea, conducted the investigations, analyzed the data, and wrote the original draft.Mesfin Belayneh Ageze: Reviewed the manuscript and edited it.The Author Contributions section has been revised to include all authors, including Mesfin Belayneh Ageze.All authors have read and approved the final manuscript.

Acknowledgement

I would like to express my sincere gratitude to Prof. Xiao Yu Yang, Dr. Yi Lu, and Dr. Ying Dong for their valuable insights and constructive feedback, which significantly improved this work.

Availability of data and materials

Data will be made available on request.

References

1. Baek, Y., C. Kim, D. K. Seo, T. Kim, J. S. Lee, Y. H. Kim, K. H. Ahn, S. S. Bae, S. C. Lee and J. Lim (2014). "High performance and antifouling vertically aligned carbon nanotube membrane for water purification." Journal of membrane Science 460: 171–177.
2. Bulbula, S. T., Y. Dong, Y. Lu and X.-Y. Yang (2018). "Graphene oxide coating enhances adsorption of lead ions on mesoporous SiO2 spheres." Chemistry Letters 47(2): 210–212.
3. Dong, Y., J. Li, L. Shi, X. Wang, Z. Guo and W. Liu (2014). "Underwater superoleophobic graphene oxide coated meshes for the separation of oil and water." Chemical communications 50(42): 5586–5589.
4. He, Z., W. Que, J. Chen, Y. He and G. Wang (2013). "Surface chemical analysis on the carbon-doped mesoporous TiO2 photocatalysts after post-thermal treatment: XPS and FTIR characterization." Journal of Physics and Chemistry of Solids 74(7): 924–928.
5. Hummers Jr, W. S. and R. E. Offeman (1958). "Preparation of graphitic oxide." Journal of the american chemical society 80(6): 1339–1339.
6. Jo, S. and Y. Kim (2016). "Superhydrophilic–underwater superoleophobic TiO 2-coated mesh for separation of oil from oily seawater/wastewater." Korean Journal of Chemical Engineering 33: 3203–3206.

7. Kang, H., Z. Cheng, H. Lai, H. Ma, Y. Liu, X. Mai, Y. Wang, Q. Shao, L. Xiang and X. Guo (2018). "Superlyophobic anti-corrosive and self-cleaning titania robust mesh membrane with enhanced oil/water separation." Separation and Purification Technology 201: 193–204.
8. Liu, M., Y. Hou, J. Li, L. Tie, Y. Peng and Z. Guo (2017). "Inorganic adhesives for robust, self-healing, superhydrophobic surfaces." Journal of Materials Chemistry A 5(36): 19297–19305.
9. Liu, Y., H. Lu, Y. Li, H. Xu, Z. Pan, P. Dai, H. Wang and Q. Yang (2021). "A review of treatment technologies for produced water in offshore oil and gas fields." Science of the Total Environment 775: 145485.
10. Lu, Y., X. Cheng, G. Tian, H. Zhao, L. He, J. Hu, S.-M. Wu, Y. Dong, G.-G. Chang and S. Lenaerts (2018). "Hierarchical CdS/m-TiO2/G ternary photocatalyst for highly active visible light-induced hydrogen production from water splitting with high stability." Nano Energy 47: 8–17.
11. Meng, C., Y. Li, Q. He, Y. Hao, W. Yin, H. Zhou and P. Li (2026). "Preparation of C and Co co-doped TiO2 Nanomaterials for Visible-Light Photocatalytic Antibacterial Activity." Water, Air, & Soil Pollution 237(13): 750.
12. Mir, S., A. Naderifar, A. morad Rahidi and M. Alaei (2022). "Recent advances in oil/water separation using nanomaterial-based filtration methods for crude oil processing-a review." Journal of Petroleum Science and Engineering 215: 110617.
13. Munirasu, S., M. A. Haija and F. Banat (2016). "Use of membrane technology for oil field and refinery produced water treatment—A review." Process safety and environmental protection 100: 183–202.
14. Nascimben Santos, E., A. Agoston, S. Kertész, C. Hodúr, Z. László, Z. Pap, Z. Kása, T. Alapi, S. G. Krishnan and G. Arthanareeswaran (2020). "Investigation of the applicability of TiO2, BiVO4, and WO3 nanomaterials for advanced photocatalytic membranes used for oil-in-water emulsion separation." Asia-Pacific Journal of Chemical Engineering 15(5): e2549.
15. Panda, S. R. and S. De (2015). "Preparation, characterization and antifouling properties of polyacrylonitrile/polyurethane blend membranes for water purification." RSC Advances 5(30): 23599–23612.
16. Reyes-Ortega, F. (2014). pH-responsive polymers: properties, synthesis and applications. Smart polymers and their applications, Elsevier: 45–92.
17. Sagadevan, S., K. Pal, P. Koteeswari and A. Subashini (2017). "Synthesis and characterization of TiO 2/graphene oxide nanocomposite." Journal of Materials Science: Materials in Electronics 28: 7892–7898.
18. Wang, R., J. Li, H. Zhou, S. Liu, W. Sun and C. Zhang (2023). "Research advancement on magnetic nanomaterial demulsifier for oil-water separation." Journal of Environmental Chemical Engineering 11(5): 110245.
19. Wen, Q., J. Di, L. Jiang, J. Yu and R. Xu (2013). "Zeolite-coated mesh film for efficient oil–water separation." Chemical Science 4(2): 591–595.
20. Xu, C., Y. Xu and J. Zhu (2014). "Photocatalytic antifouling graphene oxide-mediated hierarchical filtration membranes with potential applications on water purification." ACS applied materials &

interfaces 6(18): 16117–16123.

21. Xue, Z., S. Wang, L. Lin, L. Chen, M. Liu, L. Feng and L. Jiang (2011). "A novel superhydrophilic and underwater superoleophobic hydrogel-coated mesh for oil/water separation." Advanced Materials 37(23): 4270–4273.
22. Yang, K., B. Chen, X. Zhu and B. Xing (2016). "Aggregation, adsorption, and morphological transformation of graphene oxide in aqueous solutions containing different metal cations." Environmental science & technology 50(20): 11066–11075.
23. Zhang, H., X. Lv, Y. Li, Y. Wang and J. Li (2010). "P25-graphene composite as a high performance photocatalyst." ACS nano 4(1): 380–386.
24. Zhu, H., D. Chen, N. Li, Q. Xu, H. Li, J. He and J. Lu (2017). "Dual-layer copper mesh for integrated oil-water separation and water purification." Applied Catalysis B: Environmental 200: 594–600.

Figures

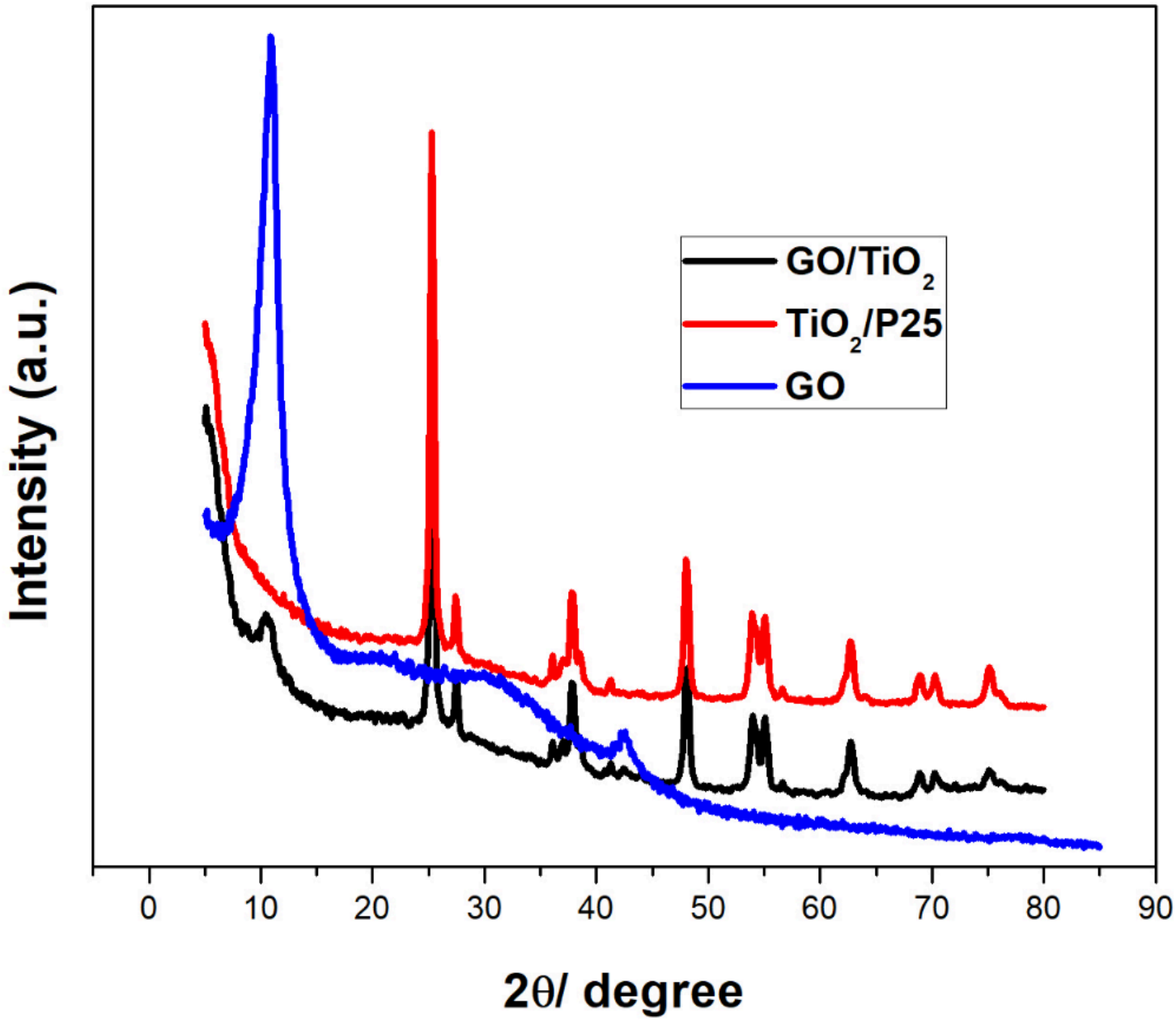


Figure 1

XRD pattern of GO, TiO_2/P25 and GO/TiO_2.

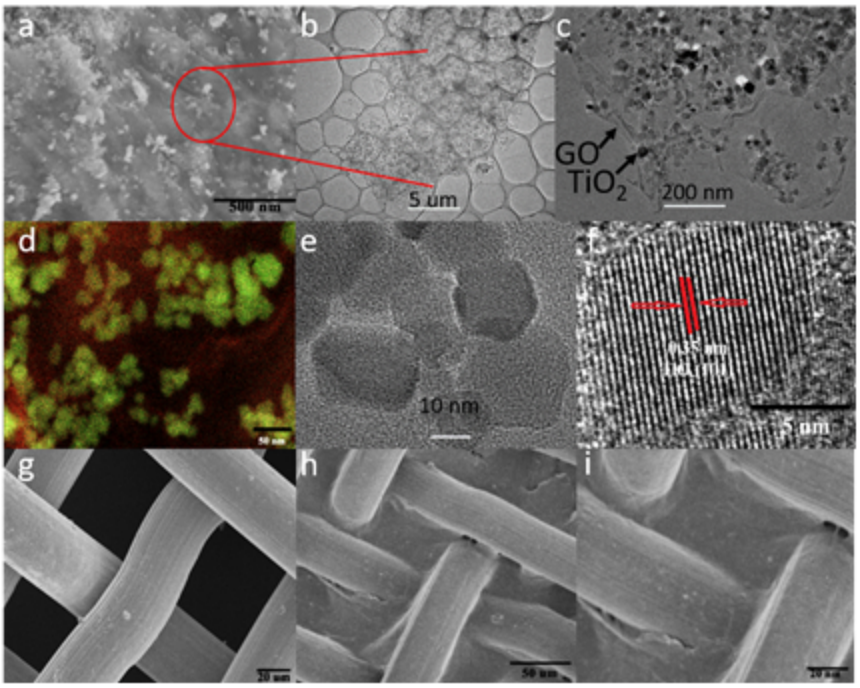


Figure 2

SEM (a), HRTEM (b-f, at different resolution magnification) images of GO/TiO_2. SEM image of (g) neat pure and (h and i) coated stainless steel meshes.

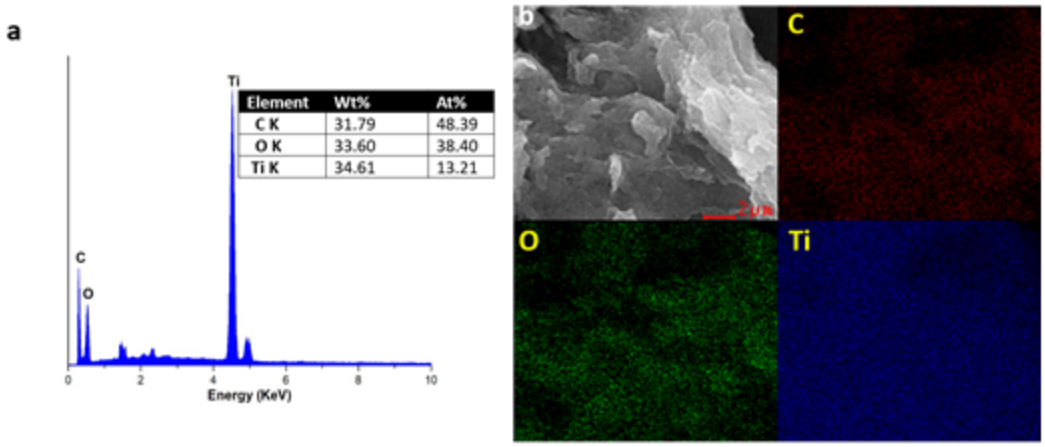


Figure 3

(a) The EDS data plot, (b) the SEM image of GO/TiO_2 with the elements mapping image of carbon (C), oxygen (O) and titanium (Ti).

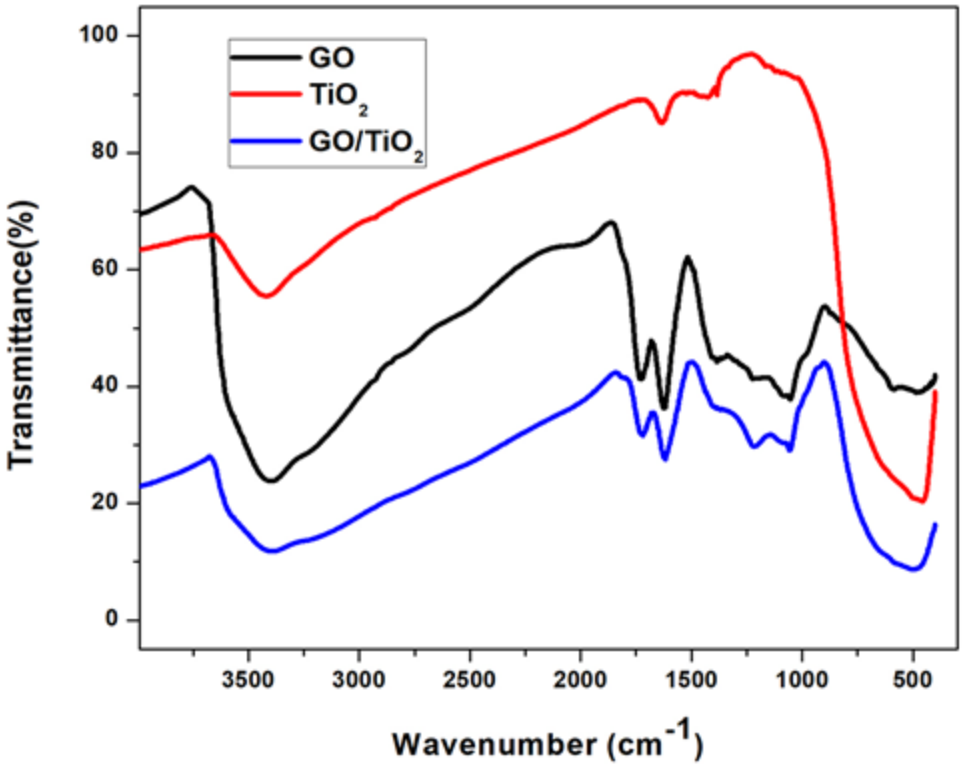


Figure 4

FTIR spectrum of GO, TiO_2 and GO/TiO_2.

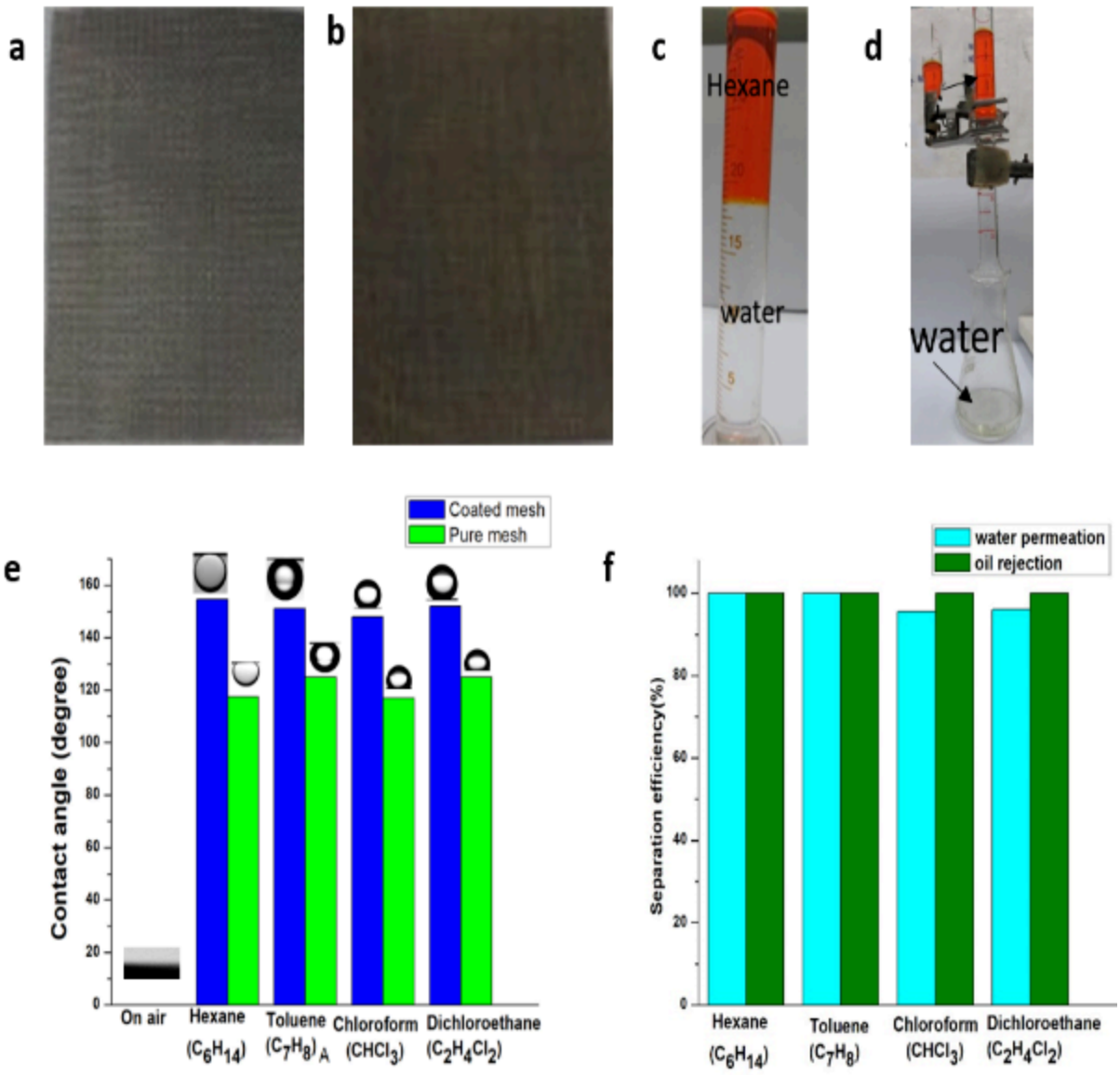


Figure 5

Photograph image of neat pure (a) and coated (b) stainless steel meshes, (c) before (d) after oil-water mixture separation (Hexane was utilized as a representative oil, while red dye was added for improved visibility.). (e) Underwater oil contact angles of hexane, toluene, chloroform, and dichloroethane. (f) The separation efficiency of the GO/TiO_2 coated mesh was evaluated for different oils based on water permeation and oil rejection.

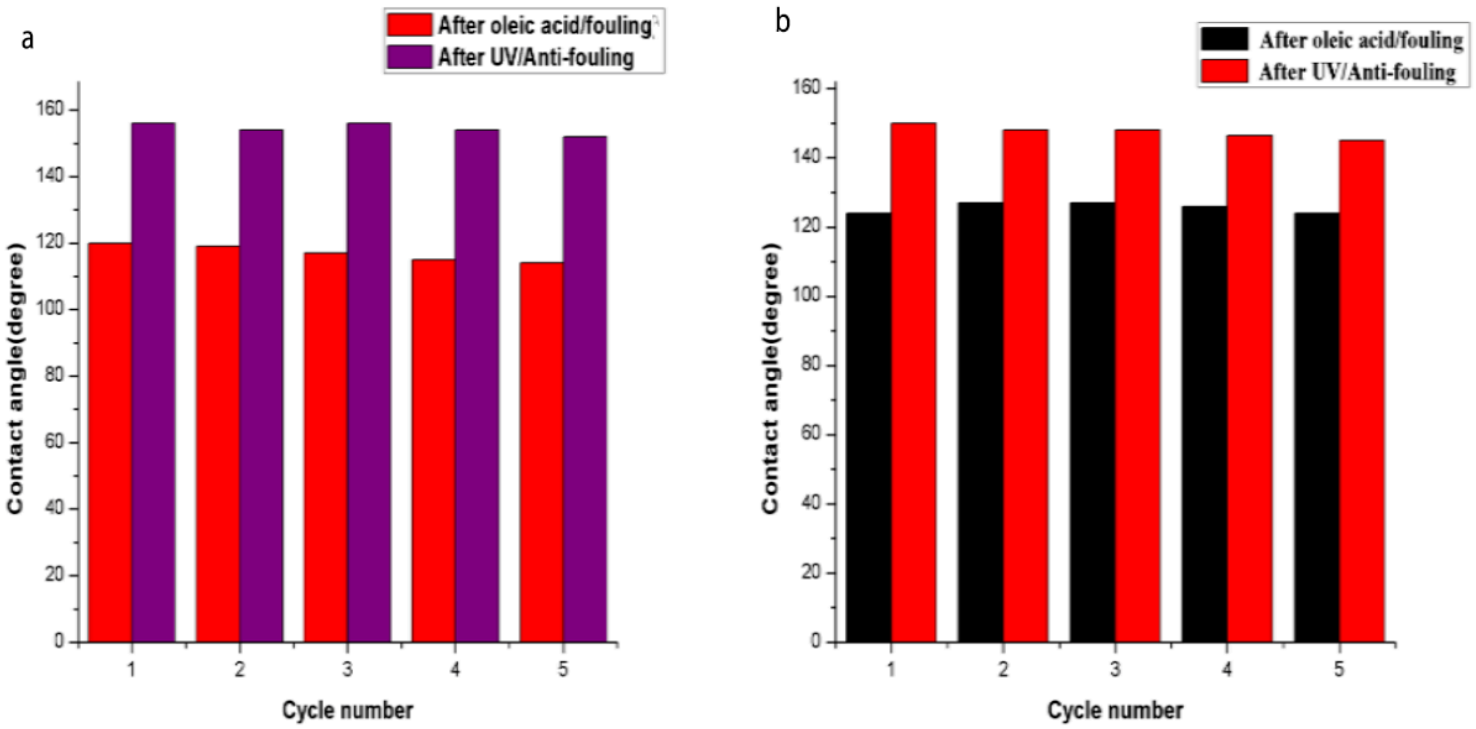


Figure 6

Fouling and anti-fouling underwater oil-contact angle measurement at different cycle number of (a) Hexane (lighter oil), (b) dichloroethane (heavier oil).